

# $\Xi(1690)^-$ production in the $K^-p \rightarrow K^+K^-\Lambda$ reaction process near threshold

Jung Keun Ahn<sup>1</sup> and Seung-il Nam<sup>2,3</sup>

<sup>1</sup>*Department of Physics, Korea University, Seoul 02841, Republic of Korea*

<sup>2</sup>*Department of Physics and Institute for Radiation Science & Technology (IRST),*

*Pukyong National University (PKNU), Busan 608-737, Republic of Korea*

<sup>3</sup>*Asia Pacific Center for Theoretical Physics (APCTP), Pohang 790-784, Republic of Korea*

(Dated: November 28, 2018)

We investigate  $\Xi(1690)^-$  production from the  $K^-p \rightarrow K^+K^-\Lambda$  reaction within the effective Lagrangian approach at the tree-level Born approximation. We consider the  $s$ - and  $u$ -channel  $\Sigma/\Lambda$  ground states and resonances for the  $\Xi$ -pole contributions, in addition to the  $s$ -channel  $\Lambda$ ,  $u$ -channel nucleon pole, and  $t$ -channel  $K^-$ -exchange for the  $\phi$ -pole contributions. The  $\Xi$ -pole includes  $\Xi(1320)$ ,  $\Xi(1535)$ ,  $\Xi(1690)(J^P = 1/2^-)$ , and  $\Xi(1820)(J^P = 3/2^-)$ . We calculate the Dalitz plot density of  $(d^2\sigma/dM_{K^+K^-}dM_{K^-\Lambda})$  at 4.2 GeV/ $c$  and the total cross sections for the  $K^-p \rightarrow K^+K^-\Lambda$  reaction near the threshold. The calculation results are in good agreement with previously acquired experimental data. Using the parameters from the fit, we present the total and differential cross sections for the two-body  $K^-p \rightarrow K^+\Xi(1690)^-$  reaction near the threshold. In our calculation, a strong enhancement at backward  $K^+$  angles is predicted because of the dominant  $u$ -channel contribution. We also demonstrate that the Dalitz plot analysis for  $p_{K^-} = 1.915 - -2.065$  GeV/ $c$  enables us to access direct information regarding  $\Xi(1690)^-$  production, which can be tested by future  $K^-$  beam experiments. The possible spin-parity states of  $\Xi(1690)^-$  are briefly discussed as well.

PACS numbers: 13.60.Le, 13.60.Rj, 14.20.Jn, 14.20.Pt

## I. INTRODUCTION

While most low-lying baryons fit primarily into SU(3) multiplets, the  $\Xi$  spectrum is still far from being established. In the  $S = -2$  sector, only the ground octet and decuplet states,  $\Xi(1320)(J^P = 1/2^+)$  and  $\Xi(1530)(J^P = 3/2^+)$ , are well-established with four-star ratings [1]. Three-star states include  $\Xi(1690)^-$ ,  $\Xi(1820)(J^P = 3/2^-)$ ,  $\Xi(1950)$ , and  $\Xi(2030)$ . The third state of  $\Xi$  has not yet been confirmed between  $\Xi(1620)$  and  $\Xi(1690)^-$ , and theoretical model predictions are still controversial [2–8]. The existence of  $\Xi(1620)$  near  $\Lambda\bar{K}$  is dubious and requires further experimental confirmation with higher statistics.

$\Xi(1690)^-$  is near the  $\Sigma\bar{K}$  threshold, and its existence has been firmly established by several experiments [9–12]. Recently, the BaBar Collaboration [13] reported that  $J = 1/2$  assignment was favored for  $\Xi(1690)^-$  from its decay angular distribution. The  $\Xi(1690)^0$  was reconstructed from  $\Lambda K_S^0$  in the  $\Lambda_c^+ \rightarrow \Lambda K_S^0 K^+$  decay, taking into account possible interference with  $a_0(980)^+$  decaying to  $K_S^0 K^+$ . Nevertheless, its spin and parity have not yet been unambiguously determined.

$\Xi(1820)$  is the only state for which spin-parity is determined ( $3/2^-$ ). The ordinary quark models predict that  $3/2^-$  and  $1/2^-$  should be almost degenerate, as in the case of  $N^*$ . Recall that  $\Lambda(1405)$  lies near  $\bar{K}N$  and it has a large mass difference ( $\approx 100$  MeV) from the doublet  $\Lambda(1520)$ . Therefore, either of  $\Xi(1620)$  or  $\Xi^*(1690)^-$  can be a spin partner of  $\Xi(1820)$ , and the rest can be regarded as an  $S = -2$  analogue state of  $\Lambda(1405)$ , namely  $\Lambda\bar{K}$  or  $\Sigma\bar{K}$  molecular states [6].

Experimentally,  $\Lambda_c^+ \rightarrow \Lambda K_S^0 K^+$  is particularly attractive, as high-statistics data are available from Belle/Belle-II and LHCb Collaborations. However, the interference between  $\Xi(1690)^-$  and  $a_0(980)$  appears with a fixed crossing location in the phase space. The phase in the interference between the two reso-

nances could change the spin analysis result.

In this respect, it is necessary to carry out a  $\Xi(1690)^-$  production experiment using the  $(K^-, K^+)$  reaction near the threshold.  $\Xi(1690)^-$  is produced in the  $(K^-, K^+)$  reaction and decays to  $\Lambda K^-$ . In the  $K^-p \rightarrow K^+K^-\Lambda$  reaction, the  $\phi(1020) \rightarrow K^+K^-$  amplitude could interfere with the  $\Xi(1690)^-$  production amplitude. However, the  $\phi(1020)$  resonance is very narrow, so it can readily be isolated from the  $\Xi(1690)^-$  resonance. Moreover, the relative location of the interference region can change with the  $K^-$  beam momentum.

For the  $K^-p \rightarrow K^+K^-\Lambda$  reaction, there have been no experimental efforts since the era of the bubble chamber. Moreover, bubble chamber data are also very limited near the threshold. Schlein *et al.* [14] reported the first measurement of the  $K^-p \rightarrow K^+K^-\Lambda$  reaction using a 1.95 GeV/ $c$   $K^-$  beam with a 72-in hydrogen bubble chamber. They observed only 24 events for  $K^-p \rightarrow K^+K^-\Lambda$  and studied the  $\phi$  resonance only. Badier *et al.* studied the  $K^-p \rightarrow K^+K^-\Lambda$  reaction using a 3 GeV/ $c$   $K^-$  beam with an 81-cm hydrogen bubble chamber [15]. Because of very limited statistics, no resonances were found in the  $\Lambda K^-$  mass spectrum. Bellefon *et al.* [16] reported total cross sections for the  $K^-p \rightarrow K^+K^-\Lambda$  reaction from 1.934 to 2.516 GeV/ $c$ . A total of 271 events were recorded in a 2-m hydrogen bubble chamber. The highest statistics data are available from the  $K^-p$  experiment at 4.2 GeV/ $c$ , involving 2935 events from a 2-m hydrogen bubble chamber [17]. The Dalitz plot for the  $K^-p \rightarrow K^+K^-\Lambda$  reaction is available. It is therefore crucial to perform a high-statistics experiment involving  $\Xi^*$  production with a high-intensity  $K^-$  beam and its decay distribution measurement to firmly determine their spin and parity; this type of experiment is possible at the J-PARC facility.

In this paper, we report numerical calculation results for the production of  $\Xi(1690)^-$  from the  $K^-p \rightarrow K^+K^-\Lambda$  reaction within the effective Lagrangian approach. We con-

$(M, J^P)$	$\Lambda(1116, 1/2^+)$	$\Lambda(1405, 1/2^-)$	$\Lambda(1520, 3/2^-)$	$\Lambda(1670, 1/2^-)$	$\Sigma(1193, 1/2^+)$	$\Sigma(1385, 3/2^+)$
$N(938, 1/2^+)$	-13.24 [22]	0.91 [21]	-10.90 [1]	0.30 [20]	3.58 [22]	-3.22 [21]
$\Xi(1322, 1/2^+)$	3.52 [22]	0.91 [21]	3.27 [21]	-0.18 [20]	-13.26 [22]	-3.22 [21]
$\Xi(1532, 3/2^+)$	4.08	-	-	-	3.22	-
$\Xi(1690, 1/2^-)$	-0.3 [8]	-	-	-	1.8 [8]	-
$\Xi(1820, 3/2^-)$	6.10 [5]	-	-	-	8.00 [5]	-

TABLE I. Coupling constants for  $KBB$  and  $K\mathcal{B}\mathcal{B}$  vertices in the present calculation are taken from Refs. [1, 5, 8, 20–22].

sider low-lying  $\Sigma/\Lambda$  resonances in  $s$ - and  $u$ -channels for the  $\Xi$ -pole contributions, and  $s$ -channel  $\Lambda$ ,  $u$ -channel nucleon pole, and  $t$ -channel  $K^-$ -exchange processes for the  $\phi$ -pole contributions. The  $\Xi$ -pole includes four  $\Xi$  states:  $\Xi(1320)$ ,  $\Xi(1535)$ ,  $\Xi(1690)(J^P = 1/2^-)$ , and  $\Xi(1820)(J^P = 3/2^-)$ . We calculate the total and differential cross sections for the  $K^-p \rightarrow \Xi(1690)^-K^+$  reaction in a beam momentum range from 2.1 GeV/ $c$  to 2.3 GeV/ $c$ . We also demonstrate that the Dalitz plot analysis of the  $K^-p \rightarrow K^+K^-\Lambda$  reaction enables us to access direct information concerning the  $\Xi(1690)^-$  production. The double-polarization asymmetry turns out to be essential for determining the spin and parity quantum numbers of  $\Xi(1690)^-$  via experiments.

## II. THEORETICAL FRAMEWORK

In this Section, we introduce the theoretical formalism to calculate the  $\Xi^*(1690)^-$  production in the  $K^-p \rightarrow K^+K^-\Lambda$  reaction within the effective Lagrangian approach at the tree-level Born approximation. We consider five relevant Feynman diagrams for the  $K^-p \rightarrow K^+K^-\Lambda$  reaction with the  $\Xi$ - and  $\phi$ -pole contributions, as shown in Fig. 1.

For the  $K^-p \rightarrow K^+K^-\Lambda$  reaction, the  $s$ - and  $u$ -channel diagrams are taken into account for the  $\Xi$  production. Four  $\Lambda$  states ( $\Lambda(1116)(J^P = 1/2^+)$ ,  $\Lambda(1405)(J^P = 1/2^-)$ ,  $\Lambda(1520)(J^P = 3/2^-)$ , and  $\Lambda(1670)(J^P = 1/2^-)$ ) and two  $\Sigma$  states ( $\Sigma(1192)(J^P = 1/2^+)$  and  $\Sigma(1385)(J^P = 3/2^+)$ ) are included in the present calculation for  $s$ - and  $u$ -channel contributions. For the  $\Xi$  production, four  $\Xi$  states ( $\Xi(1322)(J^P = 1/2^+)$ ,  $\Xi(1532)(J^P = 3/2^+)$ ,  $\Xi(1690)(J^P = 1/2^-)$ , and  $\Xi(1820)(J^P = 3/2^-)$ ) are considered for the  $\Lambda K^-$  decay channel. The Feynman diagrams for the  $\Xi$ -pole are represented in Fig. 1(a) and (b). Because the final state contains a  $K^+K^-$  pair, the  $\phi(1020)$  production can contribute to the  $K^-p \rightarrow K^+K^-\Lambda$  reaction. For the  $\phi$  production,  $s$ -channel  $\Lambda$ ,  $u$ -channel proton, and  $t$ -channel  $K^-$  exchange diagrams are included in the calculation, as shown in Fig. 1(c), (d) and (e).

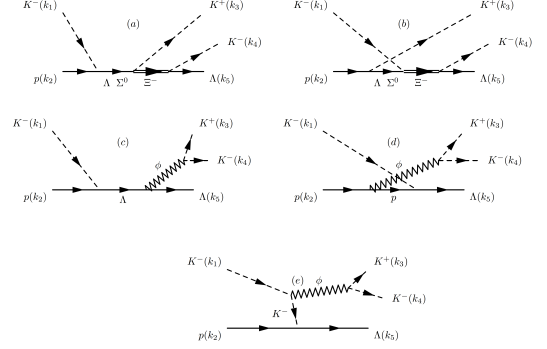


FIG. 1. Feynman diagrams for the  $K^-p \rightarrow K^+K^-\Lambda$  reaction at the tree-level Born approximation. Diagrams (a) and (b) contributed to the  $\Xi$ -pole, whereas (c), (d), and (e) contributed to the  $\phi$ -pole. The intermediate  $\Lambda/\Sigma^0/\Xi^-$  denote the ground-states as well as the resonances.

Here, we assume that the  $\Xi(1690)^-$  has a spin-parity of  $J^P = 1/2^-$ , as suggested by theoretical works [5, 8] and reported by the BaBar Collaboration [13]. To compute the invariant amplitudes for the  $K^-p \rightarrow K^+K^-\Lambda$  reaction, we use the effective Lagrangian densities for the interaction vertices as follows:

$$\mathcal{L}_{KBB} = -ig_{M_{BB}}(\bar{B}\Gamma)(\gamma_5 K)(\Gamma B), \quad (1)$$

$$\mathcal{L}_{K\mathcal{B}\mathcal{B}} = \frac{g_{K\mathcal{B}\mathcal{B}}}{M_K}(\bar{\mathcal{B}}_\mu \Gamma \gamma_5)(\gamma_5 \partial^\mu K)(\Gamma \mathcal{B}), \quad (2)$$

$$\mathcal{L}_{\phi KK} = -ig_{KK\phi} \phi^\mu [(\partial_\mu K^\dagger)K - (\partial_\mu K)K^\dagger] + \text{h.c.}, \quad (3)$$

$$\mathcal{L}_{\phi BB} = -g_{\phi BB} \bar{B} \left[ \gamma^\mu - \frac{\kappa_{\phi BB}}{2M_B} \sigma_{\mu\nu} \partial^\nu \right] \phi_\mu^* B + \text{h.c.}, \quad (4)$$

where  $B$  and  $\mathcal{B}$  stand for baryons with spin-1/2 and spin-3/2, respectively. We should mention that, in the present calculation, we did not consider the  $K\mathcal{B}\mathcal{B}$  vertex for brevity, as there are no experimental data available for this reaction.

We define  $\Gamma$ , which depends on the parity  $P$  of the neighboring baryon in the above interaction Lagrangian densities,

i.e.,  $(\Gamma B)$  and  $(\Gamma \mathcal{B})$  for instance, as follows:

$$\Gamma = \begin{cases} \mathbf{1}_{4 \times 4} & \text{for } P_{B,\mathcal{B}} = +1 \\ \gamma_5 & \text{for } P_{B,\mathcal{B}} = -1. \end{cases} \quad (5)$$

The calculation of the invariant amplitudes is straightforward:

$$i\mathcal{M}_s^{\Xi_1 Y_1} = -g_{K\Lambda\Xi_1} g_{KY_1\Xi_1} g_{KNY_1} F_{\Xi}(s) \times \frac{\bar{u}_\Lambda \gamma_5 \Gamma_{\Xi_1}(\not{q}_{4+5} + M_{\Xi_1}) \Gamma_{\Xi_1} \gamma_5 \Gamma_{Y_1}(\not{q}_{1+2} + M_{Y_1}) \Gamma_{Y_1} \gamma_5 u_N}{[M_{K^-\Lambda}^2 - M_{\Xi_1}^2 + i\Gamma_{\Xi_1} M_{\Xi_1}][s - M_{Y_1}^2 + i\Gamma_{Y_1} M_{Y_1}]}, \quad (6)$$

$$i\mathcal{M}_u^{\Xi_1 Y_1} = -g_{K\Lambda\Xi_1} g_{KY_1\Xi_1} g_{KNY_1} F_{\Xi}(u) \times \frac{\bar{u}_\Lambda \gamma_5 \Gamma_{\Xi_1}(\not{q}_{4+5} + M_{\Xi_1}) \Gamma_{\Xi_1} \gamma_5 \Gamma_{Y_1}(\not{q}_{2-3} + M_{Y_1}) \Gamma_{Y_1} \gamma_5 u_N}{[M_{K^-\Lambda}^2 - M_{\Xi_1}^2 + i\Gamma_{\Xi_1} M_{\Xi_1}][u - M_{Y_1}^2 + i\Gamma_{Y_1} M_{Y_1}]}, \quad (7)$$

$$i\mathcal{M}_s^{\Xi_3 Y_1} = \frac{g_{K\Lambda\Xi_3} g_{K\Xi_3 Y_1} g_{KNY_1} F_{\Xi}(s)}{s} \times \frac{\bar{u}_\Lambda \Gamma_{\Xi_3}(\not{q}_{4+5} + M_{\Xi_3}) \Gamma_{\Xi_3} \Gamma_{Y_1}(\not{q}_{1+2} + M_{Y_1})(k_3 \cdot k_4) \Gamma_{Y_1} \gamma_5 u_N}{[M_{K^-\Lambda}^2 - M_{\Xi_3}^2 + i\Gamma_{\Xi_3} M_{\Xi_3}][s - M_{Y_1}^2 + i\Gamma_{Y_1} M_{Y_1}]}, \quad (8)$$

$$i\mathcal{M}_u^{\Xi_3 Y_1} = \frac{g_{K\Lambda\Xi_3} g_{K\Xi_3 Y_1} g_{KNY_1} F_{\Xi}(u)}{s} \times \frac{\bar{u}_\Lambda \Gamma_{\Xi_3}(\not{q}_{4+5} + M_{\Xi_3}) \Gamma_{\Xi_3} \Gamma_{Y_1}(\not{q}_{2-3} + M_{Y_1})(k_1 \cdot k_4) \Gamma_{Y_1} \gamma_5 u_N}{[M_{K^-\Lambda}^2 - M_{\Xi_3}^2 + i\Gamma_{\Xi_3} M_{\Xi_3}][u - M_{Y_1}^2 + i\Gamma_{Y_1} M_{Y_1}]}, \quad (9)$$

$$i\mathcal{M}_s^\phi = g_{\phi KK} g_{\phi\Lambda\Lambda} g_{KN\Lambda} F_\phi(s) \times \frac{\bar{u}_\Lambda [\not{q}_{3-4}] (\not{q}_{1+2} + M_Y) \gamma_5 u_p}{[M_{K^+K^-}^2 - M_\phi^2 + i\Gamma_\phi M_\phi][s - M_Y^2 + i\Gamma_Y M_Y]}, \quad (10)$$

$$i\mathcal{M}_u^\phi = -g_{\phi KK} g_{KNY} g_{\phi NN} F_\phi(u) \times \frac{\bar{u}_\Lambda \gamma_5 (\not{q}_{5-1} + M_N) \not{q}_{3-4} u_p}{[M_{K^+K^-}^2 - M_\phi^2 + i\Gamma_\phi M_\phi][u - M_N^2]}, \quad (11)$$

$$i\mathcal{M}_t^\phi = g_{\phi KK}^2 g_{KN\Lambda} F_\phi(t) \times \frac{2(k_1 \cdot q_{3-4}) \bar{u}_\Lambda \gamma_5 u_p}{[M_{K^+K^-}^2 - M_\phi^2 + i\Gamma_\phi M_\phi][t - M_K^2]}, \quad (12)$$

where  $M_{K^+K^-} \equiv (k_3 + k_4)^2$  and  $M_{K^-\Lambda} \equiv (k_4 + k_5)^2$  denote the invariant masses. In the present calculation, the four-momenta of  $K^-$  beam, target  $p$ , outgoing  $K^+$ , outgoing  $K^-$ , and  $\Lambda$  are denoted  $k_1, k_2, k_3, k_4$ , and  $k_5$ , respectively, as shown in Fig. 1, while  $q_{i\pm j} = k_i \pm k_j$  are the relative four-momenta for two particles, where  $i$  and  $j$  range from 1 to 5.

The coupling constants for the ground-state hadron vertices, such as  $g_{KN\Lambda(1116)}$ , are taken from the prediction of the Nijmegen soft-core potential model (NSC97a) [22]. The coupling constants for the  $s$ -wave resonances,  $\Lambda(1405)$  and  $\Lambda(1670)$ , are obtained from the chiral unitary model [21], where the resonances are generated dynamically by the coupled-channel method with the Weinberg–Tomozawa (WT) chiral interaction. The couplings for  $\Xi(1690)$  and  $\Xi(1820)$  are estimated by ChUM [8] and the SU(6) relativistic quark model [5], respectively.

Regarding the coupling constants with two hyperon resonances, such as  $g_{K\Lambda^*\Xi^*}$  and  $g_{K\Sigma^*\Xi^*}$ , there is no experimental nor theoretical information available. Furthermore, it is also difficult and uncertain to simply employ the flavor SU(3)-symmetry relation, which is used to obtain  $g_{K\Lambda^*\Xi}$  and  $g_{K\Sigma^*\Xi}$  as in Ref. [20]. Hence, we set those coupling constants to be zero for simplicity, although in practice their unknown contributions can be absorbed into the cutoff parameters of the form factors. The strong coupling constants used in the present calculation are listed in Table I.

The full decay widths for  $\Xi^*$  resonances are given as  $\Gamma_{\Xi(1532)} = 9.1$  MeV [1],  $\Gamma_{\Xi(1690)} = 6$  MeV [8], and  $\Gamma_{\Xi(1820)} = 24$  MeV [1, 5]. In Eq. (6), we introduce the phenomenological form factors for the  $\Xi$ - and  $\phi$ -pole contributions to take their

spatial distributions into account:

$$F_{\Xi,\phi}(x) = \frac{\Lambda_{\Xi,\phi}^4}{\Lambda_{\Xi,\phi}^4 + (x - M_x^2)^2}, \quad \text{for } x = (s, u, t), \quad (13)$$

where  $s, t$ , and  $u$  are the Lorentz-invariant Mandelstam variables. In the present calculation, the cutoff parameters are determined to be  $\Lambda_{\Xi(1322)} = 1.3$  GeV,  $\Lambda_{\Xi(1532)} = 1.3$  GeV,  $\Lambda_{\Xi(1690)} = 0.75$  GeV,  $\Lambda_{\Xi(1820)} = 1.1$  GeV, and  $\Lambda_\phi = 0.44$  GeV to reproduce the experimental data, which will be discussed in the next Section. We also choose the phenomenological phase factors,  $e^{3i\pi/2}$  and  $e^{i\pi/2}$  for the amplitudes with the spin-1/2 and spin-3/2  $\Xi$  hyperons, respectively, as follows:

$$i\mathcal{M}_{\text{total}} = ie^{i\pi/2} \mathcal{M}_{\Xi_{3/2}} + ie^{i3\pi/2} \mathcal{M}_{\Xi_{1/2}} + i\mathcal{M}_\phi \quad (14)$$

### III. NUMERICAL RESULTS FOR THE $K^-p \rightarrow K^+K^-\Lambda$ REACTION

In this Section, we discuss the numerical results for the  $\Xi(1690)$  production. We first show the numerical results for the  $K^-p \rightarrow K^+K^-\Lambda$  reaction. The calculated Dalitz plot for the double differential cross section  $d^2\sigma/dM_{K^+K^-} dM_{K^-\Lambda}$  at  $p_{K^-} = 4.2$  GeV/ $c$  ( $E_{\text{cm}} = 3.01$  GeV) is represented in Fig. 2(a), where the  $\Xi^*(1690)$  and  $\Xi(1820)$  resonances appear as vertical bands, while  $\phi(1020)$  appears as a horizontal band in the bottom side. At this energy, there is no interference effect between  $\Xi^*$ s and  $\phi(1020)$ .

The Dalitz plot was projected on the  $K^-\Lambda$  mass axis, as shown in Fig. 2(b). The experimental data are taken from

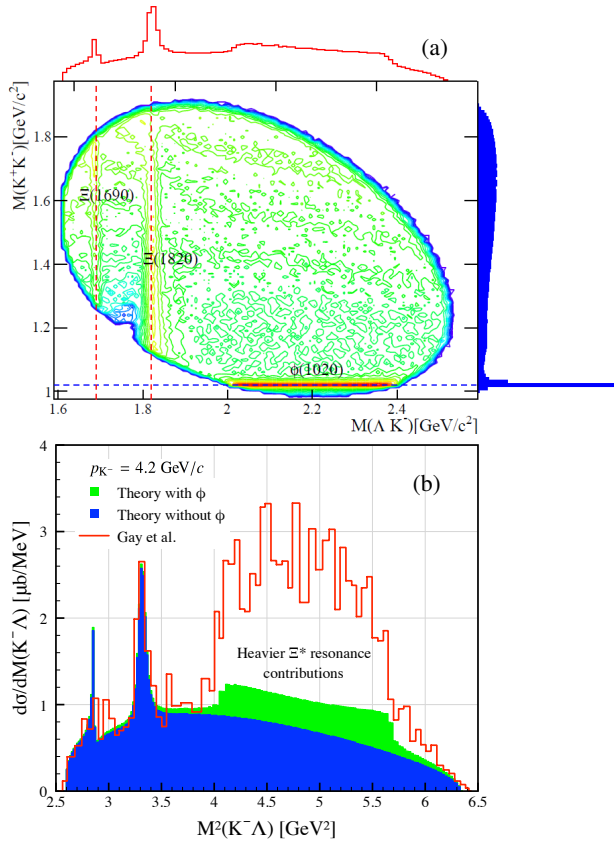


FIG. 2. (Color online) (a) Calculated Dalitz plot density ( $d^2\sigma/dM_{K^+K^-}dM_{K^-\Lambda}$ ) for the  $K^-p \rightarrow K^+K^-\Lambda$  reaction at  $p_{K^-} = 4.2$  GeV. (b) Differential cross section  $d\sigma/dM_{K^-\Lambda}$  as a function of the invariant mass squared  $M_{K^-\Lambda}^2$  at  $p_{K^-} = 4.2$  GeV. The green and blue areas indicate the results with and without the  $\phi(1020)$  contribution, respectively. The experimental data [17] are overlaid as a histogram.

Ref. [17], which is the only data set available so far for the  $K^-p \rightarrow K^+K^-\Lambda$  reaction. The experiment was performed using the  $K^-$  beam at 4.2 GeV/c to study  $\Xi(1820)$  and higher resonances. We then fit the data with the line shape of our calculation result in the low-mass region below  $M_{K^-\Lambda}^2 = 3.3$  GeV $^2/c^4$ . The first bump structure near the threshold is due to the  $\Xi(1690)$  production, providing us with information on the cutoff parameters for the form factors, as given in the previous Section. The green and blue areas indicate the calculation results with and without the  $\phi(1020)$  contribution, respectively. The mass range between 4.0 and 5.7 GeV $^2/c^4$  for the large bump structure is consistent with the  $\phi(1020)$  band crossing the limited phase space in the Dalitz plot. It should be noted that high-mass resonances decaying to  $K^-K^+$  cannot account for the bump structure in that mass range only. In the present calculation, high-mass  $K^-K^+$  resonance like  $f_2'(1525)(J^P = 2^+)$  is not included. Higher-mass  $\Xi^*$  resonances could contribute to the bump structure.

Using the same cutoff parameters, we compute the total cross sections for the  $K^-p \rightarrow K^+K^-\Lambda$  reaction. The calculation results with (green area) and without (blue area) the  $\phi(1020)$  contribution are compared with the world data taken

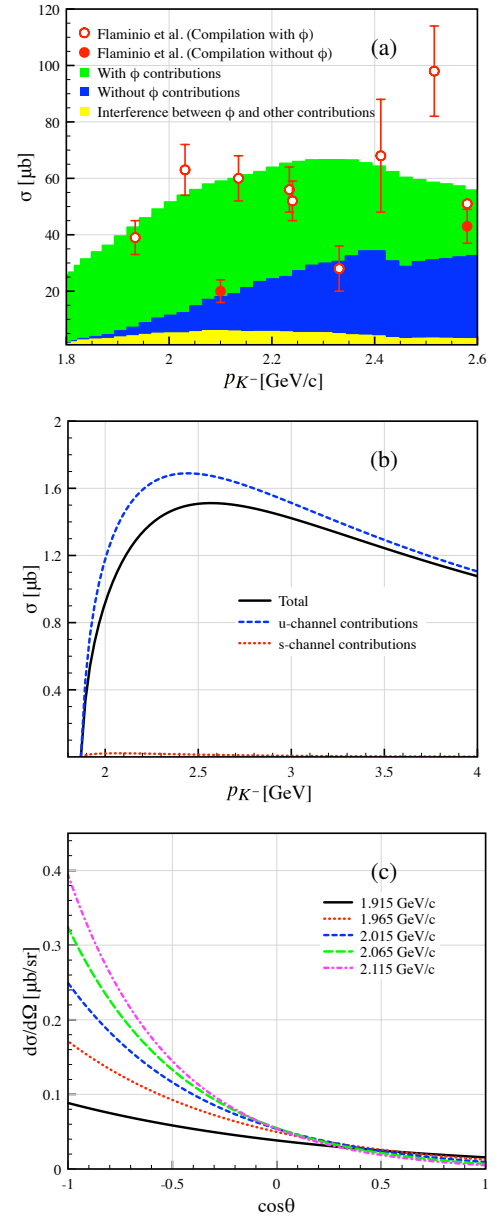


FIG. 3. (Color online) (a) Total cross section for  $K^-p \rightarrow K^+K^-\Lambda$  with (green) and without (blue)  $\phi(1020)$  contribution as functions of  $p_{K^-}$ . The yellow area at the bottom indicates interference between the  $\phi$  and other contributions. The experimental data are taken from Ref. [24]. (b) Total cross section for  $K^-p \rightarrow K^+\Xi(1690)^-$  as functions of  $p_{K^-}$ . (c) Differential cross section for  $K^-p \rightarrow K^+\Xi(1690)^-$  as functions of the angle for the outgoing  $K^+$  in the c.m. frame for several beam momenta  $p_{K^-}$ .

from Ref. [24], as shown in Fig. 3(a). The yellow area at the bottom indicates interference between the  $\phi$  and other contributions. It turns out that our theoretical model describes the experimental data for the  $K^-p \rightarrow K^+K^-\Lambda$  reaction qualitatively well. Enhanced  $K^-\Lambda$  production between  $M_{K^-\Lambda}^2 = 4.0$  GeV $^2/c^4$  and 5.7 GeV $^2/c^4$  could be associated with a contribution from higher-mass hyperon resonances. However, we

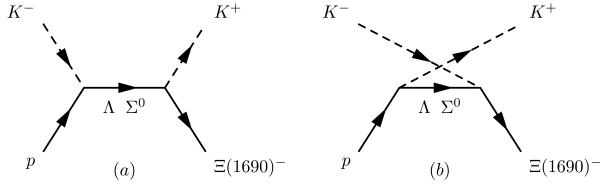


FIG. 4. Relevant Feynman diagrams for  $K^- p \rightarrow K^+ \Xi(1690)^-$ .

did not include those high-mass resonances in our present calculation, as the mass region is far beyond the  $\Lambda K^-$  threshold.

For the two-body  $K^- p \rightarrow K^+ \Xi(1690)^-$  reaction, we computed the  $s$ -channel and  $u$ -channel diagrams in Fig. 4 with the same theoretical framework and the same parameters used for the  $K^- p \rightarrow K^+ K^- \Lambda$  reaction. The total cross sections are represented as a function of  $K^-$  beam momentum ( $p_{K^-}$ ) from threshold to 4 GeV/c in Fig. 3(b). It increases rapidly from the threshold and peaks at  $p_{K^-} = 2.6$  GeV/c ( $E_{\text{cm}} = 2.47$  GeV) with  $1.5 \mu\text{b}$ , after which it decreases smoothly. As shown in Fig. 3(b), the  $u$ -channel contribution is much larger than the  $s$ -channel contribution. In our present calculation, we set the coupling constant ( $g_{KY^*\Xi^*}$ ) to zero to avoid further theoretical uncertainty. Shyam *et al.* [20] assumed that  $g_{KY^*\Xi} = g_{KY^*N}$  for the  $K^- p \rightarrow K^+ \Xi^-$  reaction. However, there is no firmly established theoretical basis for the coupling constants ( $g_{KY^*\Xi^*}$ ). The  $u$ -channel hyperon propagator and form factors also provide much larger strengths than that for the  $s$ -channel one, as previously shown in Ref. [23].

The differential cross sections  $d\sigma/d\Omega$  for the  $K^- p \rightarrow K^+ \Xi(1690)^-$  reaction are calculated as a function of  $\cos\theta$  in Fig. 3(c), where  $\theta$  stands for the scattering angle of the outgoing  $K^+$  in the center-of-mass (c.m.) frame. Because of the strong  $u$ -channel contributions, one observes backward-enhanced angular distributions for the various  $p_{K^-}$  values, as the energy increases. This backward-peaking behavior is a general feature for the double-charge and double-strangeness exchange ( $K^-, K^+$ ) process.

The threshold beam momentum for the  $K^- p \rightarrow K^+ K^- \Lambda$  reaction is 1.687 GeV/c, while that for the  $K^- p \rightarrow K^+ \Xi(1690)^-$  reaction is 1.878 GeV/c, which is accessible using the J-PARC Hadron-Hall Collaboration. The experiment for the  $K^- p \rightarrow K^+ K^- \Lambda$  reaction near the threshold can be performed with the Hyperon Spectrometer [25] at the K1.8 beam line of J-PARC. One can measure all the charged particles not only from the  $\Xi(1690)^- \rightarrow K^- \Lambda$  decay, but also  $\Sigma^- K^0$ ,  $\Sigma^0 K^-$ ,  $\Xi^- \pi^0$ , and  $\Xi^0 \pi^-$  decays. All the  $\Xi(1690)^-$  decay modes contain three charged particles with one missing neutral particle in some channels, which enables us to reconstruct  $\Xi(1690)^-$  without any kinematical ambiguity.

The sizable cross sections of a few  $\mu\text{b}$  for the  $K^- p \rightarrow K^+ \Xi(1690)^-$  reaction also encourage future experiments using a high-intensity  $K^-$  beam [26]. According to the calculated Dalitz plot density, simulated events for the  $K^- p \rightarrow K^+ K^- \Lambda$  reaction are generated over the phase space available. We assume a uniform experimental acceptance for the  $K^+ K^- \Lambda$  phase space. The Dalitz plots for the  $K^- p \rightarrow K^+ K^- \Lambda$  reaction are plotted in Fig. 5 for four different  $K^-$  beam momenta,

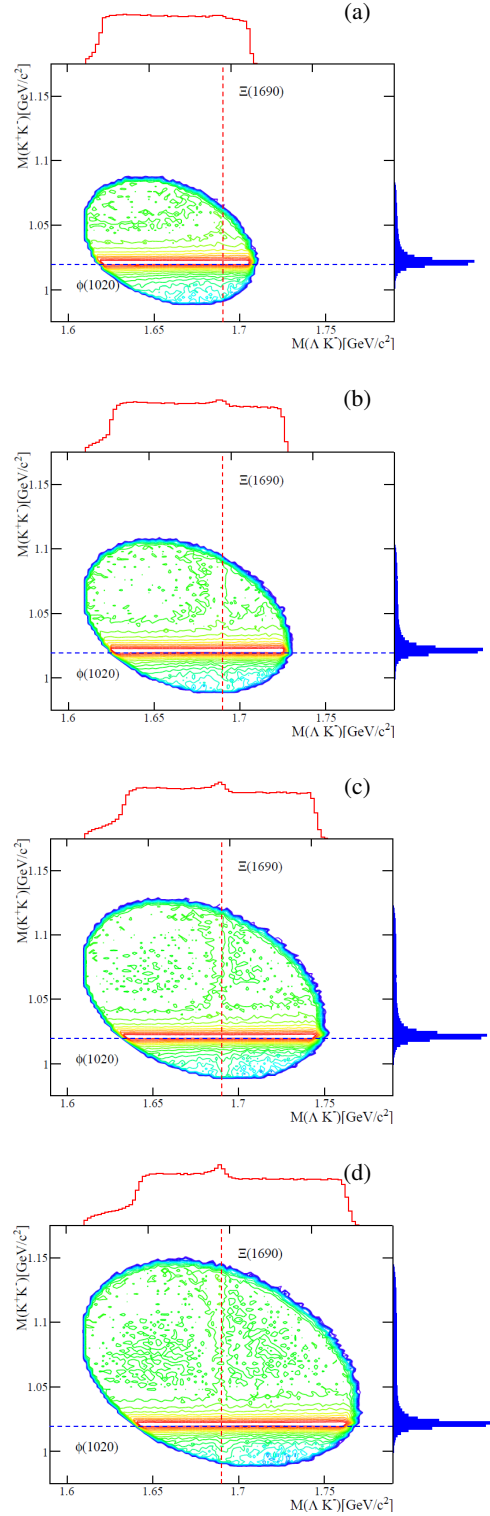


FIG. 5. (Color online) Dalitz plots for the  $K^- p \rightarrow K^+ K^- \Lambda$  reaction for (a)  $p_{K^-}^{\text{lab}} = 1.915$  GeV/c, (b) 1.965 GeV/c, (c) 2.015 GeV/c and (d) 2.065 GeV/c, respectively. The Dalitz plots are projected onto the  $\Lambda K^-$  and the  $K^+ K^-$  mass axes and plotted as histograms on the top and right sides, respectively.

from 1.915 GeV/c to 2.065 GeV/c. Because the  $\phi(1020)$  production is predominant, it is difficult to identify  $\Xi(1690)^-$  in the  $\Lambda K^-$  mass distribution without the  $\phi$ -band exclusion. The  $\phi$  band is so narrow that we can remove the  $\phi$  events by excluding the  $K^+K^-$  mass band for the  $\phi$ . The crossing points between the  $\Xi(1690)^-$  and the  $\phi(1020)$  resonances change with the  $K^-$  beam momentum. This enables us to study  $\Xi(1690)^-$  in various kinematical regions, where the interference effects with the  $\phi(1020)$  resonance are different.

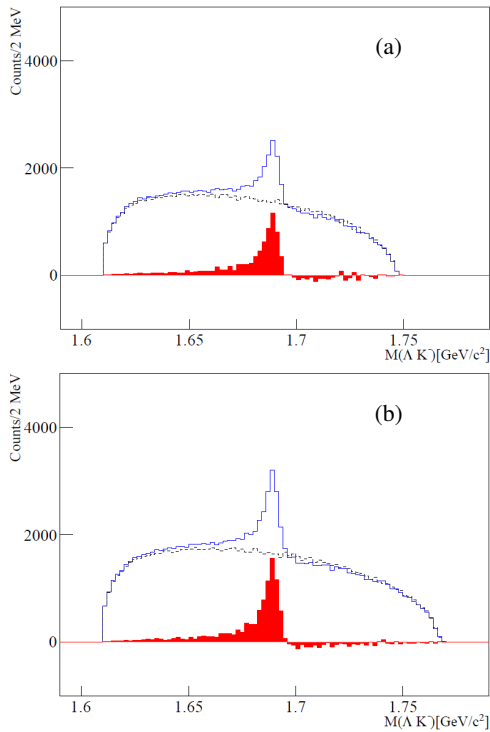


FIG. 6. (Color online) Projected  $\Lambda K^-$  mass distributions for (a)  $p_{K^-}^{\text{lab}} = 2.015$  GeV/c and (b) 2.065 GeV, respectively.

The calculated Dalitz plots show that we can neglect the interference effect between the  $\Xi(1690)^-$  and the  $\phi(1020)$  production channels in the  $K^-p \rightarrow K^+\Xi(1690)^-$  reaction. However, it is interesting to see that our theoretical model calculation predicts possible interference between the  $\Xi(1690)$  and tree-level Born-term amplitudes. Excluding the  $\phi(1020)$  band, the projected  $\Lambda K^-$  mass distributions for the beam momenta  $p_{K^-} = 2.015$  and 2.065 GeV/c are displayed in Fig. 6(a) and (b), respectively. The lineshape of the  $\Xi(1690)^-$  is clearly observed in the  $\Lambda K^-$  mass spectrum. The tree-level Born-term contribution is subtracted from the projected  $\Lambda K^-$  mass distribution, as shown with overlaid red distributions. The subtracted distributions are made of the  $\Xi(1690)^-$  and the interference effect.

Finally, we want to discuss the spin and parity of  $\Xi(1690)^-$ , which has not yet been fully determined experimentally, although the BaBar Collaboration reported that  $J^P = 1/2^-$  assignment was favored [13]. Note that the theoretical predictions also support  $J^P = 1/2^-$  [5, 8], which we have employed for the numerical results shown above. For other possible

spin-parity states, we use the following branching ratios suggested by the ChUM calculations [8], which are qualitatively consistent with experimental results [13]:

$$\frac{\Gamma_{\Xi(1690) \rightarrow \bar{K}\Lambda}}{\Gamma_{\Xi(1690)}} = 0.271, \quad \frac{\Gamma_{\Xi(1690) \rightarrow \bar{K}\Sigma}}{\Gamma_{\Xi(1690)}} = 0.533. \quad (15)$$

These values provide the relevant coupling constants as follows:

$$g_{\bar{K}\Lambda\Xi(1690)} = -(2.38, 0.90, 8.50), \\ g_{\bar{K}\Sigma\Xi(1690)} = (20.5, 7.33, 344.8) \quad (16)$$

for  $J^P = (1/2^+, 3/2^+, 3/2^-)$ , respectively. Here, we have chosen the phase factor  $-1$  between the two couplings for brevity [8]. The cutoff masses for the form factors are taken as  $\Lambda_{\Xi(1690)} = (440, 2400, 650)$  MeV, which fairly reproduce the  $K^-p \rightarrow K^+K^-\Lambda$  data [24].

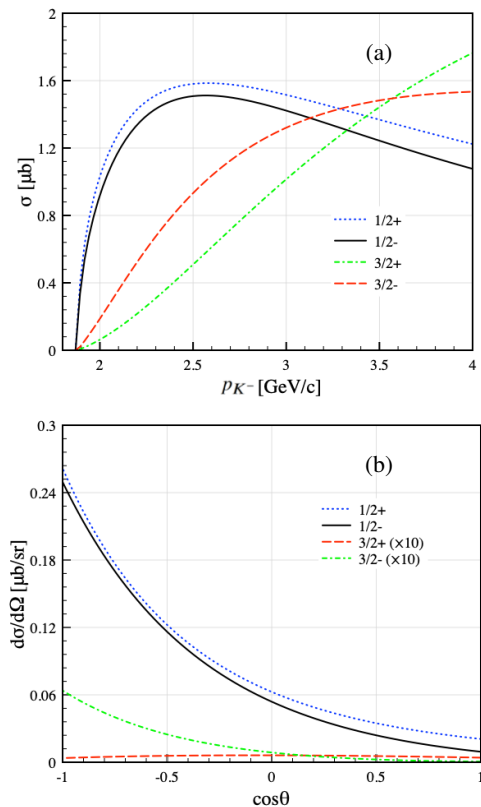


FIG. 7. (Color online) Total cross sections for  $K^-p \rightarrow K^+\Xi(1690)^-$  for different spin-parity states (a). Differential cross section for  $p_{K^-}^{\text{lab}} = 2.015$  GeV/c in the same manner (b).

In Fig. 7(a), we plot the total cross sections for  $K^-p \rightarrow K^+\Xi(1690)^-$  for different spin-parity states. The total cross sections for  $J = 1/2$  states increase rapidly near the threshold, whereas those for  $J = 3/2$  states increase smoothly due to the  $p$ -wave nature near the threshold. The differential cross sections for  $p_{K^-}^{\text{lab}} = 2.015$  GeV/c in Fig. 7(b) show a strong enhancement at backward  $K^+$  c.m. angles because of the dominant  $u$ -channel contributions for  $J = 1/2^+, 1/2^-$  and  $3/2^-$

states. For  $J = 3/2^+$  state, it turns out that the  $s$ - and  $u$ -channel contributions compete strongly with each other.

Taking into account the lack of experimental and theoretical information on those quantum numbers, it is crucial to investigate theoretically physical observables that do not depend much on theoretical uncertainties, such as the form factors and coupling constants. One of the observables satisfying this criterion is *double-polarization asymmetry* for the present case  $K^-p \rightarrow K^+\Xi(1690)^-$ , which reads:

$$\Sigma(s_R) = \frac{d\sigma_{\uparrow}/d\Omega - d\sigma_{\downarrow}/d\Omega}{d\sigma_{\uparrow}/d\Omega + d\sigma_{\downarrow}/d\Omega}. \quad (17)$$

Here, the subscripts ( $\uparrow, \downarrow$ ) denote the proton-target polarizations along a quantization axis, when the  $\Xi(1690)^-$  possesses a fixed spin state ( $s_R$ ). As understood from Eq. (17), the phenomenological form factors and coupling constants, being multiplied to the invariant amplitudes, are canceled approximately between the numerator and denominator, minimizing those theoretical uncertainties.

In Fig. 8, we plot  $\Sigma(s_R)$  for different spin-parity states of  $\Xi(1690)^-$  for  $p_{K^-}^{\text{lab}} = 2.015$  GeV/ $c$ . We chose  $J_z = +1/2$  for  $J^P = 1/2^\pm$  and summed over  $J_z = +1/2$  and  $J_z = +3/2$  contributions for  $J^P = 3/2^\pm$ . Because we do not have a meson exchange in the  $t$  channel here, the spin-conserving process dominates for  $J^P = 1/2^\pm$ , i.e.,  $\Sigma \sim 1$ , as shown in Fig. 8. Because the  $J^P = 1/2^-$  state provides sizable spin-nonconserving contributions, it differs slightly from the  $J^P = 1/2^+$  one. On the contrary, the  $J^P = 3/2^\pm$  states show both spin-nonconserving and spin-mixing contributions. Hence, from these observations, double-polarization asymmetry is a useful tool for determining the spin and parity quantum numbers of  $\Xi(1690)^-$ .

#### IV. SUMMARY

In this study, we investigate the  $\Xi(1690)^-$  production in the  $K^-p \rightarrow K^+\Xi(1690)^-$  reaction within the effective Lagrangian approach. We consider the  $s$ - and  $u$ -channel  $\Sigma/\Lambda$  ground states and resonances for the  $\Xi$ -pole contributions, in addition to the  $s$ -channel  $\Lambda$ ,  $u$ -channel nucleon pole, and  $t$ -channel  $K^-$ -exchange for the  $\phi$ -pole contributions. The  $\Xi$ -pole includes  $\Xi(1320)$ ,  $\Xi(1535)$ ,  $\Xi(1690)(J^P = 1/2^-)$ , and

$\Xi(1820)(J^P = 3/2^-)$ . We calculate the Dalitz plot density of ( $d^2\sigma/dM_{K^+K^-}dM_{K^-\Lambda}$  at 4.2 GeV/ $c$ ) and the total cross sections for the  $K^-p \rightarrow K^+K^-\Lambda$  reaction near the threshold to determine the coupling constants and the form factors for the two-body  $K^-p \rightarrow K^+\Xi(1690)^-$  reaction. The calculated differential cross sections for the  $K^-p \rightarrow K^+\Xi(1690)^-$  reaction near the threshold show a strong enhancement at backward  $K^+$  angles, caused by the dominant  $u$ -channel contribution. We also demonstrate that the Dalitz plot analysis for  $p_{K^-} = 1.915 - 2.065$  GeV/ $c$  enables us to access direct information regarding the  $\Xi(1690)^-$  production, which can be tested by future  $K^-$  beam experiments. The double-polarization asymmetry turns out to be essential to determine the spin and parity quantum numbers of  $\Xi(1690)^-$  via experiments.

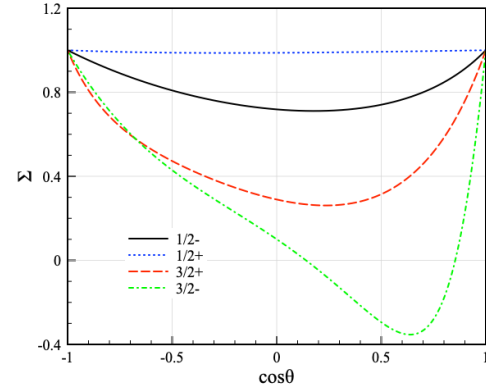


FIG. 8. (Color online) Double-polarization asymmetry  $\Sigma(s_R)$  as a function of  $\cos \theta$  for the various spin-parity states of  $\Xi(1690)^-$  for  $p_{K^-}^{\text{lab}} = 2.015$  GeV/ $c$ .

#### ACKNOWLEDGMENTS

S.i.N. is grateful to S. H. Kim (PKNU/CENuM) for fruitful discussions. The works of J.K.A. and S.i.N. were partially supported by the National Research Foundation (NRF) of Korea (No. 2018R1A5A1025563, No. 2017R1A2B2011334).

[1] M. Tanabashi *et al.* (Particle Data Group), Phys. Rev. D **98**, 030001 (2018).  
[2] A. Ramos, E. Oset and C. Bennhold, Phys. Rev. Lett. **89**, 252001 (2002).  
[3] C. Garcia-Recio, M. F. M. Lutz and J. Nieves, Phys. Lett. B **582**, 49 (2004).  
[4] Y. Oh, Phys. Rev. D **75**, 074002 (2007).  
[5] L. Y. Xiao and X. H. Zhong, Phys. Rev. D **87**, 094002 (2013).  
[6] T. Sekihara, PTEP **2015**, no. 9, 091D01 (2015).  
[7] K. Miyahara *et al.*, Phys. Rev. C **95**, 035212 (2017).  
[8] K. P. Khemchandani *et al.*, Phys. Rev. D **97**, 034005 (2018).

[9] C. Dionisi *et al.* (Amsterdam-CERN-Nijmegen-Oxford Collaboration), Phys. Lett. B **80**, 145 (1978).  
[10] S.F. Biagi *et al.*, Z. Phys. C, **9**, 305 (1981).  
[11] S.F. Biagi *et al.*, Z. Phys. C, **34**, 15 (1987).  
[12] K. Abe *et al.* (Belle Collaboration), Phys. Lett. B **524**, 33 (2002).  
[13] B. Aubert *et al.* (BaBar Collaboration), Phys. Rev. D **78**, 034008 (2008).  
[14] P. Schlein, W. E. Slater, L. T. Smith, D. H. Stork and H. K. Ticho, Phys. Rev. Lett. **10**, 368 (1963).  
[15] J. Badier *et al.*, Phys. Lett., **16**, 171 (1965).  
[16] A. de Bellefont *et al.*, Nuovo Cim. A **41**, 451 (1977).

- [17] J. B. Gay *et al.* (Amsterdam-CERN-Nijmegen-Oxford Collaboration), Phys. Lett. B **62**, 477 (1976).
- [18] J. Gasser and H. Leutwyler, Nucl. Phys. B **250**, 465 (1985).
- [19] J. S. Lindsey and G. A. Smith, Phys. Rev. **147**, 913 (1966).
- [20] R. Shyam, O. Scholten and A. W. Thomas, Phys. Rev. C **84**, 042201 (2011).
- [21] K. Nakayama, Y. Oh and H. Haberzettl, Phys. Rev. C **74**, 035205 (2006).
- [22] T. A. Rijken, V. G. J. Stoks and Y. Yamamoto, Phys. Rev. C **59**, 21 (1999).
- [23] S. i. Nam, A. Hosaka and H. C. Kim, J. Korean Phys. Soc. **52**, 561 (2008).
- [24] V. Flaminio, W. G. Moorhead, D. R. O. Morrison and N. Rivoire, CERN-HERA-83-02.
- [25] J. K. Ahn, JPS Conf. Proc. **17**, 031104 (2017).
- [26] S. Y. Ryu, Letter of Intent for Study of Odd-Parity  $\Sigma$  and  $\Xi$  Resonances in  $K^-p$  Reactions with the Hyperon Spectrometer at J-PARC (2015).